Available online at www.sciencedirect.com
ScienceDirect
Trans. Nonferrous Met. Soc. China 34(2024) 2733−2742
Transactions of Nonferrous Metals Society of China
www.tnmsc.cn

Strength and plasticity improvement induced by strong grain refinement after Zr alloying in selective laser-melted AlSiMg1.4 alloy

Yao-xiang GENG[1], Chun-feng ZAI[1], Jiang YU[1], Hao TANG[2], Hong-wei LÜ[1], Zhi-jie ZHANG[1]

1. School of Materials Science and Engineering, Jiangsu University of Science and Technology, Zhenjiang 212100, China;
2. National Engineering Research Center of Near-Net Shape Forming for Metallic Materials, South China University of Technology, Guangzhou 510640, China

Received 15 February 2023; accepted 25 July 2023

Abstract: In order to enhance the mechanical properties of the selective laser-melted (SLM) high-Mg content AlSiMg1.4 alloy, the Zr element was introduced. The influence of Zr alloying on the processability, microstructure, and mechanical properties of the alloy was systematically investigated through performing microstructure analysis and tensile testing. It was demonstrated that the SLM-fabricated AlSiMg1.4−Zr alloy exhibited high process stability with a relative density of over 99.5% at various process parameters. Besides, the strong grain refinement induced by the primary Al_3Zr particle during the melt solidification process simultaneously enhanced both the strength and plasticity of the alloy. The values for the yield strength, ultimate tensile strength, and elongation of the SLM-fabricated AlSiMg1.4−Zr were (343±3) MPa, (485±4) MPa, and (10.2±0.2)%, respectively, demonstrating good strength−plasticity synergy in comparison to the AlSiMg1.4 and other Al−Si-based alloys fabricated by SLM.
Key words: selective laser melting; process stability; grain refinement; microstructure; mechanical properties

1 Introduction

Lightweighting is considered a crucial index for evaluating the progressiveness of aerospace vehicles [1]. The selective laser melting (SLM) technology can enable the quick, and one-time manufacturing of complex precision metal parts. Consequently, based on this technology, the mass of the parts can be effectively reduced, and the performance of the parts can be improved through topological optimization of the structure and the integrated manufacturing of multiple parts [2−4]. High-strength aluminum alloys, e.g., 2xxx and 7xxx, are commonly used in the manufacturing of key parts in aerospace vehicles. However, the wide freezing ranges render these alloys susceptible to liquation cracking and hot tearing during the implementation of the SLM process [5]. Therefore, the application of SLM-fabricated aluminum alloys is currently focused on traditional Al−Si and Al−Si−Mg alloy compositions, such as AlSi12, AlSi7Mg, and AlSi10Mg [6,7]. Unfortunately, the mechanical strength of these alloys is significantly lower than that of conventional high-strength aluminum alloys [8].

Compared with conventional manufacturing technology, the rapid cooling nature during SLM process (cooling rate of 10^5−10^8 K/s) can efficiently refine the grain size and achieve a high solid solubility of alloying elements in the matrix. As a result, the strengthing effects including fine grain

Corresponding author: Yao-xiang GENG, Fax/Tel: +86-511-84401184, E-mail: yaoxianggeng@163.com
DOI: 10.1016/S1003-6326(24)66572-6
1003-6326/© 2024 The Nonferrous Metals Society of China. Published by Elsevier Ltd & Science Press
This is an open access article under the CC BY-NC-ND license (http://creativecommons.org/licenses/by-nc-nd/4.0/)

strengthening, solid solution strengthening, and precipitation strengthening of the alloy can be significantly improved [9,10]. KIMURA et al [11] systematically studied the impact of Mg content (0−2.5 wt.%) on the processability, microstructure, and mechanical properties of the SLM-fabricated Al−4Si−Mg alloy. The results indicated that as the Mg content increased, the density and grain size of the sample gradually decreased, and the strength increased. Nevertheless, when the Mg content exceeded 2.0 wt.% the elongation of the alloy decreased rapidly. The maximum yield strength (YS) and the ultimate tensile strength (UTS) of the sample were 275 and 425 MPa, respectively, with an elongation of 5%−7%. Recently, GENG et al [12−16] reported the SLM-fabricated high Mg-content AlSi8.1Mg1.4 and AlSi8Mg3 aluminum alloys. The SLM-fabricated AlSi8.1Mg1.4 alloy exhibited good processability and mechanical properties, with a minimum porosity of 0.047%, YS of (341±14) MPa, UTS of (518±6) MPa, and an elongation of (7.1±0.4)%, respectively. Furthermore, the increase of Mg content in the SLM-fabricated Al−Si−Mg alloy resulted in the formation of Mg−Si clusters in the α-Al cells. Following the direct aging process, these Mg−Si clusters could act as precursors of the β'' phase for further precipitating and growth, thereby effectively enhancing the strength of the alloy. The SLM-fabricated AlSi8Mg3 alloy showed very high hardness and strength, with a Vickers hardness of over HV 210 and a compressive yield strength of over 540 MPa. These results were attributed to the increase in the proportion of Si-rich cell boundaries and the density of the Mg_2Si strengthening nanoparticles induced by the high content of Mg. However, the alloy almost lost its plasticity. Increasing the Mg content is an effective method for increasing the strength of the SLM-fabricated Al−Si−Mg alloy. However, the excessive Mg will significantly reduce the plasticity of the alloy. It is thus necessary to introduce alloying elements to regulate the mechanical properties of the SLM-fabricated Al−Si−Mg alloy.

The incorporation of Zr alloying elements in 2xxx and 7xxx series alloys can effectively avoid the hot cracks generated during the SLM process and improve the mechanical properties of the alloys by producing fine equiaxed grains at the boundary of the molten pool [17−19]. For instance, MARTIN et al [17] first fabricated a crack-free SLM-fabricated 7075 alloy by introducing Zr alloying elements to induce the grain refinement effect. In another interesting work, WANG et al [18] reported a high-strength, crack-free SLM-fabricated Zr-modified 2024 Al alloy with tensile properties comparable to that of wrought 2024-T651 alloy. Recently, GUO et al [20,21] fabricated a novel SLM-fabricated Er/Zr-modified Al−7Si−0.6Mg alloy. The authors demonstrated that the strength and elongation increased after Er and Zr alloying due to the grain refinement induced by the $(Al,Si)_3(Er,Zr)$ particles. From these perspectives, in this work, a novel Zr-modified, high-Mg-content AlSi8.1Mg1.4 alloy was fabricated using SLM. The results showed that the addition of Zr to the AlSi8.1Mg1.4 alloy can effectively improve the process stability, refine the grain size, and increase the mechanical properties of the alloy. Our work provides valuable guidance for improving process stability and mechanical properties of SLM-fabricated commercial Al−Si−Mg alloy.

2 Experimental

2.1 Powder material

AlSiMg1.4 and AlSiMg1.4−Zr pre-alloying powders were prepared using the vacuum induction gas atomization (VIGA) method. The chemical composition of the powder was tested by an inductively coupled plasma atomic scanning spectrometer (ICP, PE OPTIMA 7300DV). The results are listed in Table 1. The surface morphology and particle size distribution of these powders are presented in Fig. 1. The pre-alloying powders were spherical in shape (Figs. 1(a) and (b)). The average sizes (D_{50}) of the AlSiMg1.4 and AlSiMg1.4−Zr powders were 35.2 and 36.9 μm, respectively (Fig. 1(c)).

Table 1 Chemical compositions of AlSiMg1.4 and AlSiMg1.4−Zr powders (wt.%)

Powder	Si	Mg	Zr	Fe	Al
AlSiMg1.4	8.17	1.42	−	0.20	Bal.
AlSiMg1.4−Zr	7.43	1.57	0.37	0.08	Bal.

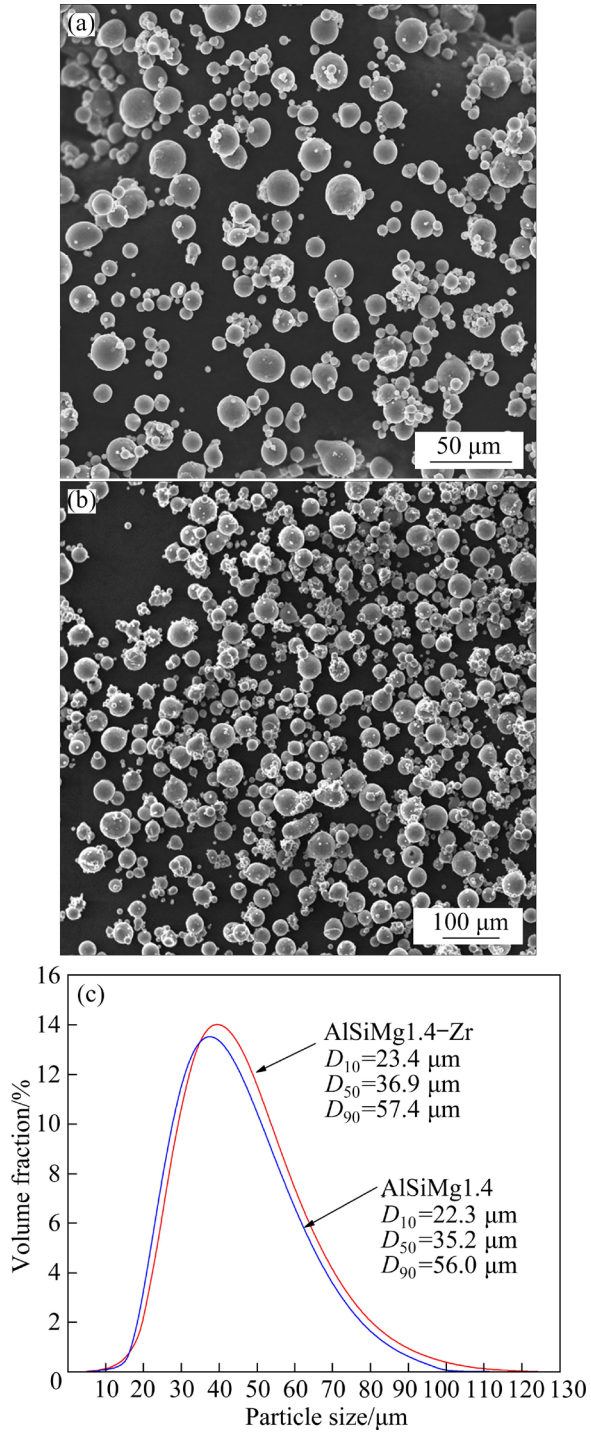

Fig. 1 SEM images (a, b) and size distribution (c) of AlSiMg1.4 (a) and AlSiMg1.4−Zr (b) powders

2.2 Specimen fabrication

The bulk specimens with a dimension of 55 mm (length) × 15 mm (width) × 16 mm (height) were fabricated using EP-M250 equipment with a spot size of 70 μm at room temperature. During the SLM process, laser powers of 250 and 350 W, spot size of 70 μm, layer thickness of 30 μm, hatch spacing of 70 μm, scanning speed of 800−1200 mm/s, and rotate angle of 67° were used. Argon gas was used to protect the powder from oxidation. The density of the SLM specimens was measured using the Archimedes method. The relative density was obtained by dividing the measured density by the theoretical density. The theoretical densities for AlSiMg1.4 and AlSiMg1.4−Zr alloys were 2.678 and 2.685 g/cm^3, respectively.

2.3 Microstructural characterization

The surface morphology of powders and microstructure of the SLM-fabricated specimens were analyzed with a scanning electron microscope (SEM, JSM−6480, at 200 kV). An optical microscope (OM, Axio Vert.A1) was used to analyze the type of hole of the specimens. The grain size and crystal orientation analysis of the specimens were carried out by electron backscatter diffraction (EBSD, OXFORD, Nordlys Nano) using a step size of 0.3 μm. The low-angle and high-angle grain settings were 2°−15° and over 15°, respectively. The transmission electron microscopy (TEM) investigations were performed on a JEM−2010F, operated at 200 kV. TEM samples were prepared by mechanical grinding to ~50 μm, and a Twin-Jet Electropolisher was used to make a thin area.

2.4 Mechanical properties

A UTM5105 universal testing machine was used to test the tensile property of the as-built alloy at a constant strain rate of 1 mm/min according to the ASTM E8-04 standard. The dimensions of the tensile sample are shown in Fig. 2. The data were the average values of three specimens. All microstructure characterization and mechanical properties tests were carried out on the specimen fabricated at a laser power of 250 W and a laser scanning speed of 1100 mm/s. All tests were carried out at room temperature.

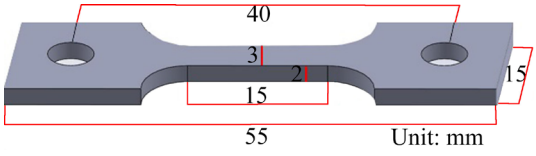

Fig. 2 Dimensions of tensile sample

3 Results and discussion

3.1 Processability

Figures 3 and 4 show the OM images of the SLM-fabricated AlSiMg1.4 and AlSiMg1.4−Zr samples under varying process parameters, respectively. Only a few metallurgical pores induced by hydrogen, metal gases, and hollow powders could be found in all samples [22]. Moreover, the change in the relative densities of the samples with the process parameters is depicted in Fig. 5. For the SLM-fabricated AlSiMg1.4 sample, the process parameters had a large impact on the relative density, with minimum and maximum relative densities of (99.07±0.16)% and (99.79±0.16)%, respectively. In contrast, the relative density of the SLM-fabricated AlSiMg1.4−Zr sample varied between 99.50% and 99.61%, showing extremely high process stability and processability. In the present alloy, the addition of Zr alloying elements can also control the laser powder bed interaction instabilities by adjusting the viscosity of the melt during the SLM process. Therefore, the fluctuation of the molten pool can be simultaneously stabilized, and the coalescence of the liquid droplets can be prevented, which could result in the elimination of large spatters and the printing of defective lean samples with good consistency [23]. In striking contrast, during the conventional SLM-fabricated aluminum alloys, the process parameters had a significant impact on the processability and properties of the alloy, resulting in unstable mechanical properties and low equipment applicability [24]. In the SLM-fabricated AlSiMg1.4−Zr alloy, the wide process parameter window is expected to significantly improve the stability of the mechanical properties of the SLM parts.

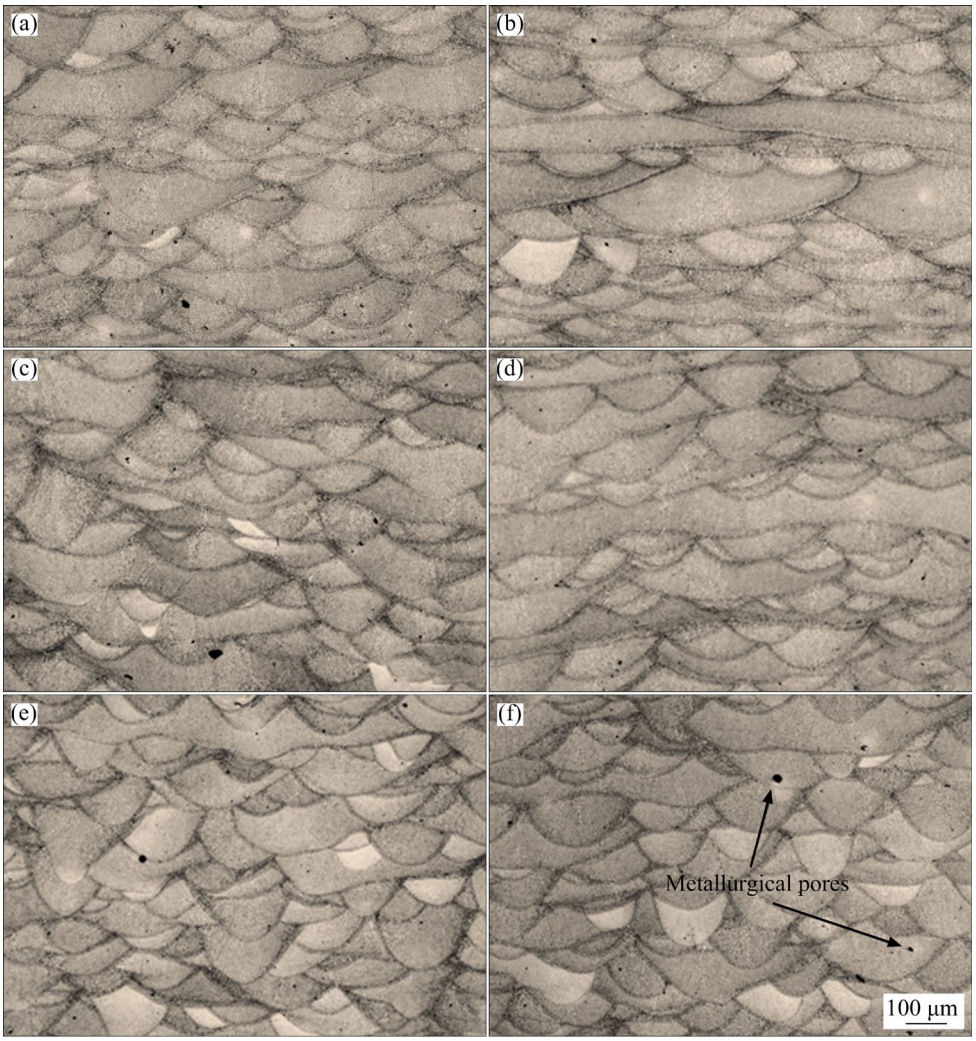

Fig. 3 OM images of AlSiMg1.4 samples fabricated under different process parameters: (a) 250 W, 800 mm/s; (b) 250 W, 1000 mm/s; (c) 250 W, 1200 mm/s; (d) 350 W, 800 mm/s; (e) 350 W, 1000 mm/s; (f) 350 W, 1200 mm/s

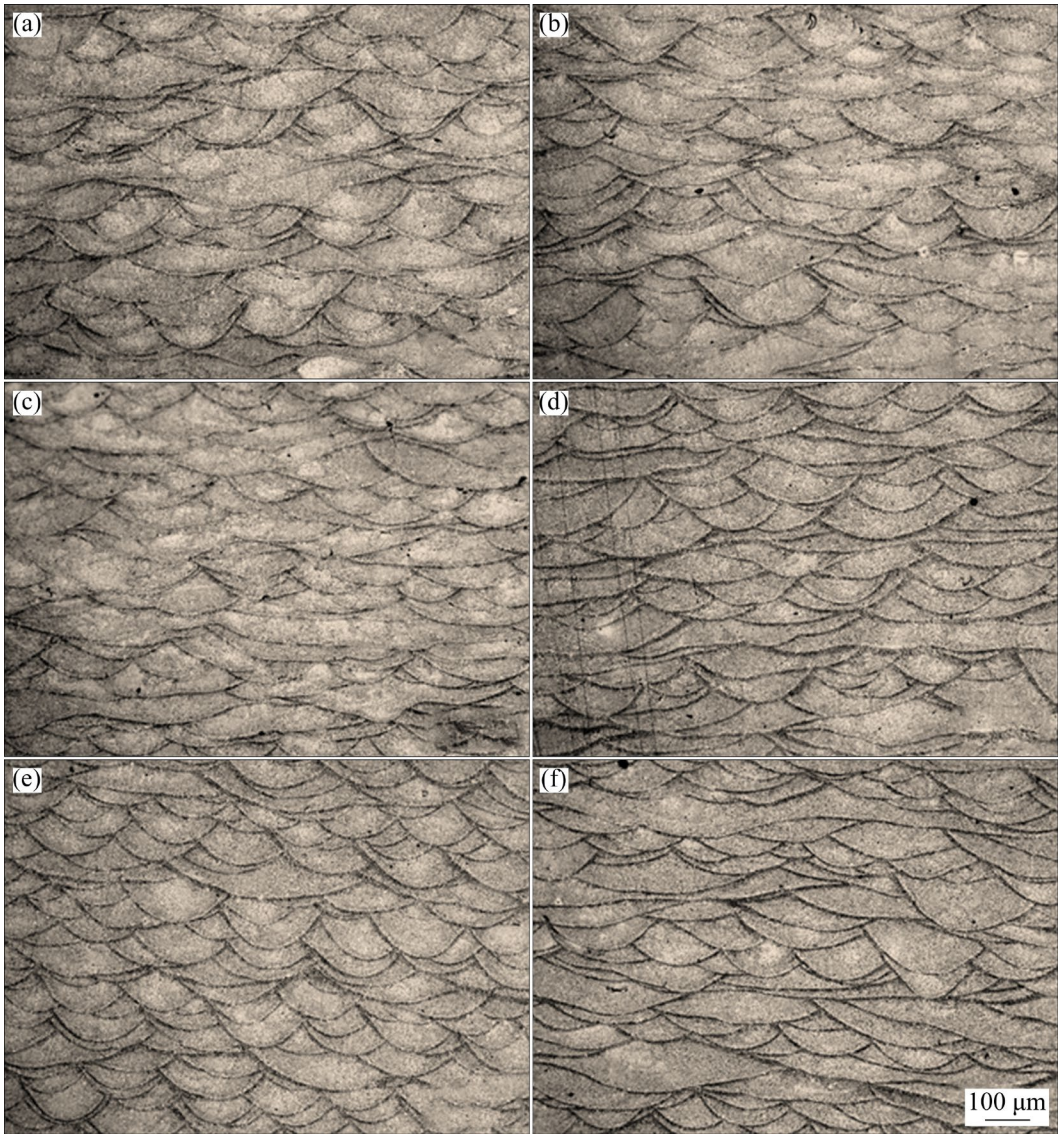

Fig. 4 OM images of AlSiMg1.4−Zr samples fabricated under different process parameters: (a) 250 W, 800 mm/s; (b) 250 W, 1000 mm/s; (c) 250 W, 1200 mm/s; (d) 350 W, 800 mm/s; (e) 350 W, 1000 mm/s; (f) 350 W, 1200 mm/s

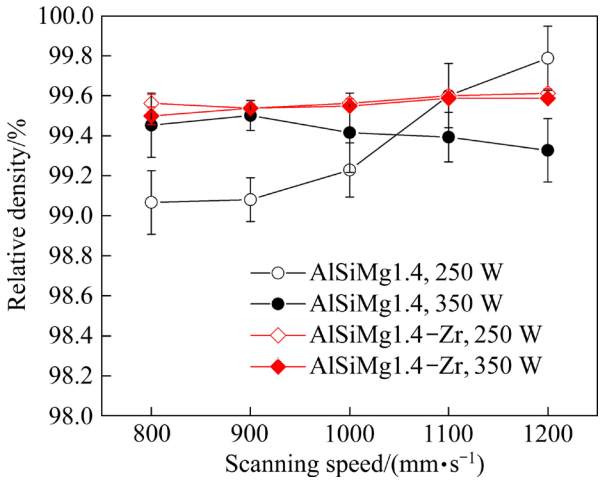

Fig. 5 Relative densities of SLM-fabricated AlSiMg1.4 and AlSiMg1.4−Zr samples

3.2 Microstructure

Figure 6 displays EBSD orientation maps and schematic representations during the implementation of the solidification process of the SLM-fabricated AlSiMg1.4 and AlSiMg1.4−Zr samples. The SLM-fabricated AlSiMg1.4 sample exhibited columnar grains primarily, with a small number of equiaxed grains located in the pool boundaries, as depicted in Figs. 6(a) and (c). The average grain size of the sample was about (7±3) μm. Conversely, an equiaxed-columnar bimodal grain structure was revealed by EBSD with a relatively large number of equiaxed grains presented in the molten pool boundaries and an average grain size of about (3±1) μm in the SLM-

fabricated AlSiMg1.4−Zr sample (Fig. 6(b)), which was similar to those of the SLM-fabricated Zr- and/or Sc-modified aluminum alloys [25−27]. In traditional cast or forged aluminum alloys, Zr is typically used as a grain refiner to combat hot-tearing and increase mechanical properties [28]. During the SLM process of the AlSiMg1.4−Zr alloys, the precipitation of the primary Al_3Zr or $(Al,Si)_3Zr$ could serve as a nucleation site for α-Al grains due to its low mismatch degree with the aluminum matrix, producing a strong grain refining effect [18,20]. As a result, a large number of small equiaxed grains with random orientation will be generated at the solidification front, i.e., the molten pool boundary (Figs. 6(b) and (d)), which could alleviate the internal stresses load generated during the SLM process, decrease the deformation of parts, and improve the processability and the mechanical properties of the alloy [25]. With the progress of the solidification, the increasing solidification front velocity led to solute trapping, which effectively suppressed the formation of grain refiners according to time-dependent nucleation theory [29]. In the absence of nuclei, the residual melt formed coarse columnar grains with a ⟨100⟩ texture along the solidification direction [30]. However, the existence of equiaxed grains could refine the size of the columnar grains because the equiaxed grains would impede the continuous growth of the columnar front [20,31], as shown in Fig. 6(b). SEM images presented in Figs. 7(a) and (b) indicate that the α-Al matrix of the SLM-fabricated AlSiMg1.4−Zr sample displayed a cellular substructure, consisting of fine and slightly coarse cell regions with a heat-affected zone located in between (Fig. 7(a)). Moreover, spherical Si nanoparticles were also precipitated from the α-Al cells, as shown in Fig. 7(b), which was similar to the other SLM-fabricated Al−Si−Mg alloys [13−15,21,32]. Additionally, the boundaries of the cells were rich in Si and Mg elements [33]. TEM analysis revealed that a large number of GP zones with a size of about 2 nm were present in the α-Al cell matrix, which can be identified by the fast Fourier transformation (FFT) pattern and the corresponding Fourier filtered image, as shown in Figs. 7(c) and (d). This phenomenon could also be observed in the SLM-fabricated AlSiMg1.4 alloy [14]. These GP zones can act as precursors for the precipitation of the β'' phase during artificial aging, and effectively improve the strength of the aging alloy [14,15].

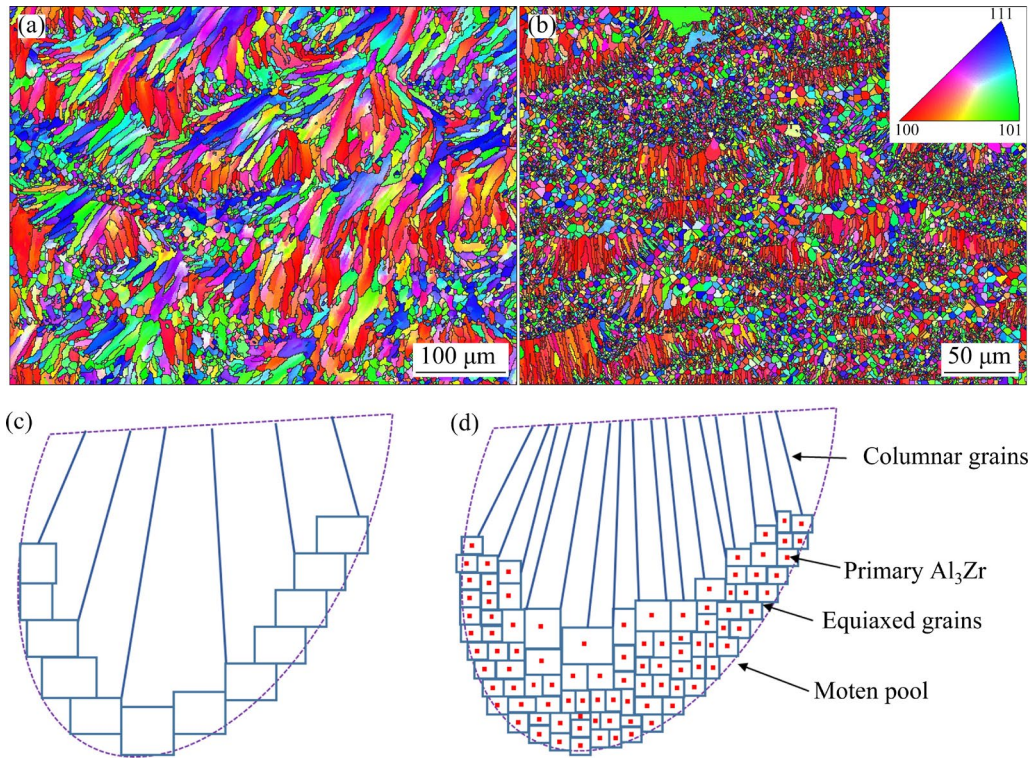

Fig. 6 EBSD orientation maps (a, b) and schematic representations during solidification process (c, d) of SLM-fabricated AlSiMg1.4 (a, c) and AlSiMg1.4−Zr (b, d) samples

3.3 Mechanical properties

Figure 8(a) shows typical engineering stress–strain curves of the SLM-fabricated AlSiMg1.4 and AlSiMg1.4−Zr alloys. The YS, UTS and elongation of the SLM-fabricated AlSiMg1.4 alloy were (295±6) MPa, (476±3) MPa, and (8.4±0.6)%, respectively. The inoculation of Zr in the AlSiMg1.4 alloy simultaneously increased the strength and plasticity with YS, UTS and elongation of (343±3) MPa, (485±4) MPa, and (10.2±0.2)%, respectively. The present SLM-fabricated AlSiMg1.4−Zr alloy exhibited good strength−plasticity synergy in comparison to the Al−Si-based alloys fabricated by SLM [11,15,33−40], as depicted in Fig. 8(b).

Zr alloying caused a significant grain refinement effect in the SLM-fabricated Al−Si−Mg alloy, which remarkably increased the tensile properties of the alloy. Particularly, the YS increased from (295±6) MPa for the AlSiMg1.4 alloy to (343±3) MPa for the AlSiMg1.4−Zr alloy. According to the Hall−Petch law, the YS due to grain boundary strengthening ($\Delta\sigma_{gb}$) can be expressed by the following expression [41]:

$$\Delta\sigma_{gb}=K(d_{Al-Zr}^{-1/2}-d_{Al}^{-1/2}) \quad (1)$$

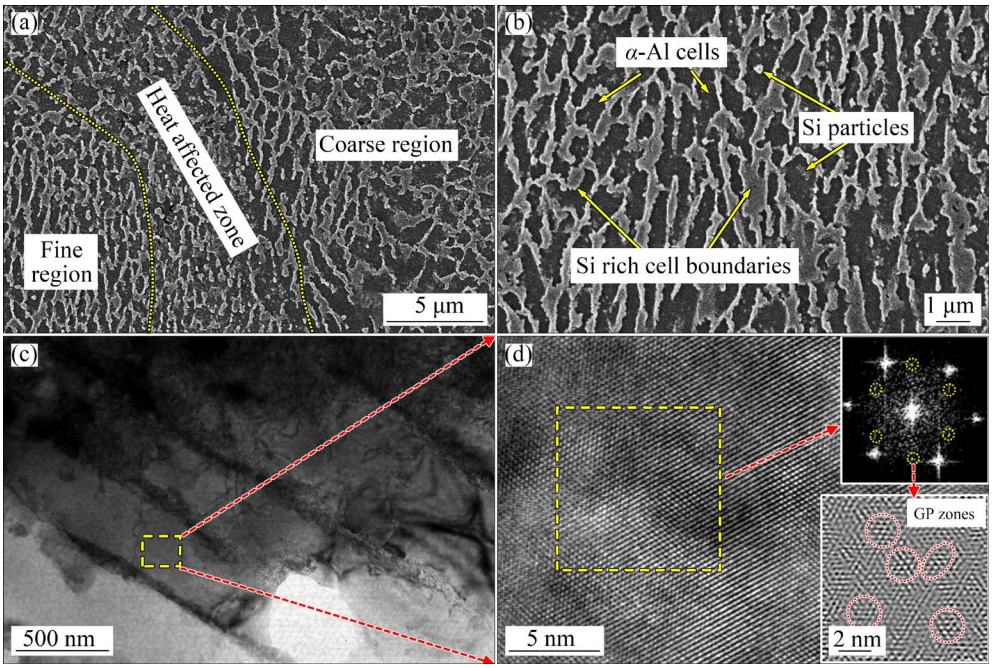

Fig. 7 SEM (a, b), TEM bright field (c), and HRTEM (d) images of SLM-fabricated AlSiMg1.4−Zr samples (The inset in Fig. 7(d) shows the FFT pattern and corresponding Fourier-filtered image produced by five spots in yellow circles of the FFT pattern)

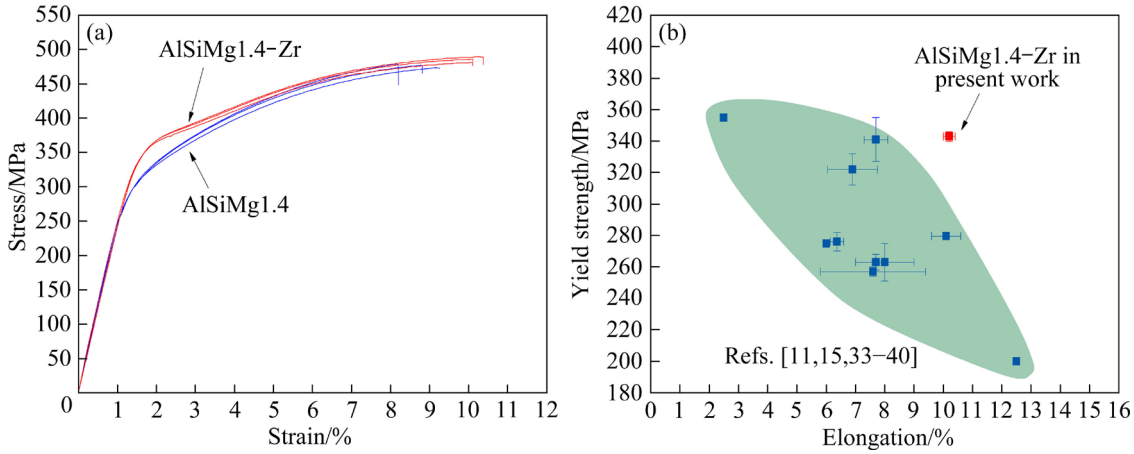

Fig. 8 Tensile stress−strain curves of SLM-fabricated AlSiMg1.4 and AlSiMg1.4−Zr samples (a) and comparison of YS and elongation of SLM-fabricated AlSiMg1.4−Zr alloy with other typical Al−Si-based alloys fabricated by SLM in their as-built state (b)

where K is a constant and can be set as 0.17 MPa·m$^{1/2}$ [19], and d_{Al-Zr} and d_{Al} represent the grain sizes of the SLM-fabricated AlSiMg1.4−Zr and AlSiMg1.4 alloys, respectively. Based on the acquired EBSD results, the average grain sizes of the SLM-fabricated AlSiMg1.4 and AlSiMg1.4−Zr alloys were 3 μm and 7 μm, respectively. Therefore, the increase in grain boundary strengthening can be calculated as ~34 MPa, which was lower than the experimental result of ~48 MPa. The remaining strength increment could be attributed to the solid-solution strengthening of the Zr atom and the higher Mg concentrations of AlSiMg1.4−Zr than those observed in the AlSiMg1.4. The contribution of the solid solution strengthening ($\Delta\sigma_{ss}$) to the YS increment can be described as follows [42]:

$$\Delta\sigma_{ss} = M\left(\frac{3}{8}\right)^{2/3}\left(\frac{1+v}{1-v}\right)^{4/3}\left(\frac{w}{b}\right)^{1/3} G\,|\varepsilon|^{4/3}\,c^{2/3} \quad (2)$$

where M is the average Taylor factor (3.06 for Al), v denotes the Poisson's ratio (0.345 for Al), w=5b, b is the magnitude of the Burgers vector, G is the shear modulus, ε is the lattice misfit strain (1.28% for Mg and 1.35% for Zr) [43], and c is the molar fraction of solute elements retained in the Al solid solution. Furthermore, according to the TEM−EDS analysis, the concentrations of Mg and Zr in α-Al for the SLM-fabricated AlSiMg1.4−Zr alloy were about 0.8 and 0.1 at.%, respectively, while the concentration of Mg in the SLM-fabricated AlSiMg1.4 alloy was about 0.4%. The estimated strength increment induced by Zr and Mg was around 12 MPa. For the SLM-fabricated AlSiMg1.4−Zr alloy, the sum of the grain boundary strengthening increment (~34 MPa) and solid solution strengthening increment (~12 MPa) results in an estimated YS of 46 MPa, which is in direct agreement with the experimental results (48 MPa).

4 Conclusions

(1) The SLM-fabricated AlSiMg1.4−Zr alloy exhibited a heterogeneous grain structure with a relatively large number of ultrafine α-Al equiaxed grains at the molten pool boundary and a small amount of columnar α-Al grains in the inner region of the molten pool. The strong grain refinement effect combined with the stabilized molten pool fluctuation induced by Zr alloying remarkably enhanced the SLM processability and process stability of the SLM-fabricated AlSiMg1.4−Zr alloy, which was expected to improve the stability of the mechanical properties of the SLM-generated parts.

(2) The ultrafine-grained microstructure mainly provided high strength and ductility in the SLM-fabricated AlSiMg1.4−Zr alloy with a YS of (343±3) MPa and an elongation of (10.2±0.2)%, exhibiting good strength−plasticity synergy.

(3) Due to the combination of good SLM processability, high process stability, and excellent mechanical properties, the SLM-fabricated AlSiMg1.4−Zr alloys displayed broad application prospects in the industry.

CRediT authorship contribution statement

Yao-xiang GENG: Methodology, Validation, Formal analysis, Investigation, Data curation, Writing − Original draft, Writing − Review & editing; **Chun-feng ZAI**, **Jiang YU**, **Hao TANG**, **Hong-wei LÜ**, and **Zhi-jie ZHANG:** Data curation.

Declaration of competing interest

The authors declare that they have no known competing financial interests or personal relationships that could have appeared to influence the work reported in this paper.

Acknowledgments

This work was supported by the National Natural Science Foundation of China (Nos. 51801079, 52001140).

References

[1] LIN Xin, HUANG Wei-dong. High performance metal additive manufacturing technology applied in aviation field [J]. Materials China, 2015, 34: 684−688. (in Chinese)

[2] GU D D, MEINERS W, WISSENBACH K, POPRAWE R. Laser additive manufacturing of metallic components: Materials, processes and mechanisms [J]. International Materials Reviews, 2012, 57: 133−164.

[3] WANG P, ECKERT J, PRASHANTH K G, WU M W, KABAN I, XI L X, SCUDINO S. A review of particulate-reinforced aluminum matrix composites fabricated by selective laser melting [J]. Transactions of Nonferrous Metals Society of China, 2020, 30: 2001−2034.

[4] YU S J, WANG P, LI H C, SETCHI R, WU M W, LIU Z Y, CHEN Z W, WAQAR S, ZHANG L C. Heterogeneous microstructure and mechanical behaviour of Al−8.3Fe−1.3V−1.8Si alloy produced by laser powder bed fusion [J]. Virtual and Physical Prototyping, 2023, 18: e2155197.

[5] TANG H, GENG Y X, BIAN S N, XU J H, ZHANG Z J. An ultra-high strength over 700 MPa in Al−Mn−Mg−Sc−Zr

alloy fabricated by selective laser melting [J]. Acta Metallurgica Sinica (English Letters), 2022, 35: 466−474.

[6] ABOULKHAIR N T, SIMONELLI M, PARRY L, ASHCROFT I, TUCK C, HAGUE R. 3D printing of aluminium alloys: Additive manufacturing of aluminium alloys using selective laser melting [J]. Progress in Materials Science, 2019, 106: 100578.

[7] QI J F, LIU C Y, CHEN Z W, LIU Z Y, TIAN J S, FENG J, OKULOV I V, ECKERT J, WANG P. Enhancement in strength and thermal stability of selective laser melted Al−12Si by introducing titanium nanoparticles [J]. Materials Science and Engineering A, 2022, 855: 143833.

[8] ZHANG D N, SHANGGUAN Q Q, XIE C J, LIU F. A modified Johnson−Cook model of dynamic tensile behaviors for 7075-T6 aluminum alloy [J]. Journal of Alloys and Compounds, 2015, 619: 186−194.

[9] TANG H, GENG Y X, LUO J J, XU J H, JU H B, YU L H. Mechanical properties of high Mg-content Al−Mg−Sc−Zr alloy fabricated by selective laser melting [J]. Metals and Materials International, 2021, 27: 2592−2599.

[10] GENG Y X, TANG H, XU J H, ZHANG Z J, XIAO Y K, WU Y. Strengthening mechanisms of high-performance Al−Mn−Mg−Sc−Zr alloy fabricated by selective laser melting [J]. Science China Materials, 2021, 64: 3131−3137.

[11] KIMURA T , NAKAMOTO T, OZAKI T, SUGITA K, MIZUNO M, ARAKI H. Microstructural formation and characterization mechanisms of selective laser melted Al−Si−Mg alloys with increasing magnesium content [J]. Materials Science and Engineering A, 2019, 754: 786−798.

[12] HOU Y, GENG Y X, CHEN J H, LUO J J, TANG H, XU J H, YU L H, JU H B. Super-hardness of $AlSiMg_3$ alloy formed by selective laser melting [J]. Rare Metal Materials and Engineering, 2020, 49: 3943−3949. (in Chinese)

[13] GENG Y X, TANG H, XU J H, HOU Y, WANG Y X, HE Z, ZHANG Z J, JU H B, YU L H. Influence of process parameters and aging treatment on the microstructure and mechanical properties of AlSi8Mg3 alloy fabricated by selective laser melting [J]. International Journal of Minerals, Metallurgy and Materials, 2022, 29: 1770−1779.

[14] GENG Y X, WANG Q, WANG Y M, ZANG Q H, MI S B, XU J H, XIAO Y K, WU Y, LUAN J H. Microstructural evolution and strengthening mechanism of high-strength AlSi8.1Mg1.4 alloy produced by selective laser melting [J]. Materials & Design, 2022, 218: 110674.

[15] GENG Y X, WANG Y M, XU J H, MI S B, FAN S M, XIAO Y K, WU Y, LUAN J H. A high-strength AlSiMg1.4 alloy fabricated by selective laser melting [J]. Journal of Alloys and Compounds, 2021, 867: 159103.

[16] GENG Yao-xiang, FAN Shi-min, JIAN Jiong-lin, XU Su, ZHANG Zhi-jie, JU Hong-bo, YU Li-hua, XU Jun-hua. Mechanical properties of AlSiMg alloy specifically designed for selective laser melting [J]. Acta Metallurgica Sinica, 2020, 56: 821−830. (in Chinese)

[17] MARTIN J H, YAHATA B D, HUNDLEY J M, MAYER J A, SCHAEDLER T A, POLLOCK T M. 3D printing of high-strength aluminium alloys [J]. Nature, 2017, 549: 365−369.

[18] WANG Y F, LIN X, KANG N, WANG Z H, WANG Q Z, LIU Y X, HUANG W D. Laser powder bed fusion of Zr-modified Al−Cu−Mg alloy: Crack-inhibiting, grain refinement, and mechanical properties [J]. Materials Science and Engineering A, 2022, 838: 142618.

[19] WANG Y F, LIN X, KANG N, WANG Z H, WANG Q Z, LIU Y X, HUANG W D. Influence of post-heat treatment on the microstructure and mechanical properties of Al−Cu−Mg−Zr alloy manufactured by selective laser melting [J]. Journal of Materials Science & Technology, 2022, 111: 35−48.

[20] GUO Y W, WEI W, HUANG H, WEN S P, SHI W, ZHOU X R, WU X L, GAO K Y, RONG L, QI P, NIE Z R. Approaching an ultrafine microstructure and excellent tensile properties of a novel Er/Zr modified Al−7Si−0.6 Mg alloy fabricated by selective laser melting [J]. Journal of Materials Research and Technology, 2023, 22: 1625−1637.

[21] GUO Y W, WEI W, SHI W, XUE D, ZHOU X R, WEN S P, WU X L, GAO K Y, HUANG H, NIE Z R. Selective laser melting of Er modified AlSi7Mg alloy: Effect of processing parameters on forming quality, microstructure and mechanical properties [J]. Materials Science and Engineering A, 2022, 842: 143085.

[22] WEINGARTEN C, BUCHBINDER D, PIRCH N, MEINERS W, WISSENBACH K, POPRAWE R. Formation and reduction of hydrogen porosity during selective laser melting of AlSi10Mg [J]. Journal of Materials Processing Technology, 2015, 221: 112−120.

[23] QU M L, GUO Q L, ESCANO L I, NABAA A, HOJJATZADEH S M H, HOJJATZADEH H, YOUNG Z A, CHEN L Y. Controlling process instability for defect lean metal additive manufacturing [J]. Nature Communications, 2022, 13: 1079.

[24] WU B, JI X Y, ZHOU J X, YANG H Q, PENG D J, WANG Z M, WU Y J, YIN Y J. In situ monitoring methods for selective laser melting additive manufacturing process based on images — A review [J]. China Foundry, 2021, 18: 265−285.

[25] CROTEAU J R, GRIFFITHS S, ROSSELL M D, LEINENBACH C, KENEL C, JANSEN V, SEIDMAN D N, DUNAND D C, VO N Q. Microstructure and mechanical properties of Al−Mg−Zr alloys processed by selective laser melting [J]. Acta Materialia, 2018, 153: 35−44.

[26] JIA Q B, ROMETSCH P, KÜRNSTEINER P, CHAO Q, HUANG A J, WEYLAND M, BOURGEOIS L, WU X H. Selective laser melting of a high strength Al−Mn−Sc alloy: Alloy design and strengthening mechanisms [J]. Acta Materialia, 2019, 171: 108−118.

[27] ZHOU L, HYER H, PARK S, PAN H, BAI Y L, RICE K P, SOHN Y. Microstructure and mechanical properties of Zr-modified aluminum alloy 5083 manufactured by laser powder bed fusion [J]. Additive Manufacturing, 2019, 28: 485−496.

[28] FULLER C B, KRAUSE A R, DUNAND D C, SEIDMAN D N. Microstructure and mechanical properties of a 5754 aluminum alloy modified by Sc and Zr additions [J]. Materials Science and Engineering A, 2002, 338: 8−16.

[29] SHAO G, TSAKIROPOULOS P. Prediction of phase selection in rapid solidification using time dependent nucleation theory [J]. Acta Metallurgica et Materialia, 1994, 42: 2937−2942.

[30] ZHANG J L, GAO J B, SONG B, ZHANG L J, HAN C J, CAI C, ZHOU K, SHI Y S. A novel crack-free Ti-modified Al−Cu−Mg alloy designed for selective laser melting [J]. Additive Manufacturing, 2021, 38: 101829.
[31] OPPRECHT M, GARANDET J P, ROUX G, FLAMENT C. An understanding of duplex microstructures encountered during high strength aluminium alloy laser beam melting processing [J]. Acta Materialia, 2021, 215: 117024.
[32] THIJS L, KEMPEN K, KRUTH J P, VAN HUMBEECK J V. Fine-structured aluminium products with controllable texture by selective laser melting of pre-alloyed AlSi10Mg powder [J]. Acta Materialia, 2013, 61: 1809−1819.
[33] RAO J H, ZHANG Y, FANG X Y, CHEN Y, WU X H, DAVIES C H J. The origins for tensile properties of selective laser melted aluminium alloy A357 [J]. Additive Manufacturing, 2017, 17: 113−122.
[34] MENEZES J T O D, CASTRODEZA E M, CASATI R. Effect of build orientation on fracture and tensile behavior of A357 Al alloy processed by selective laser melting [J]. Materials Science and Engineering A, 2019, 766: 138392.
[35] BAI Y C, YANG Y Q, XIAO Z F, ZHANG M K WANG D. Process optimization and mechanical property evolution of AlSiMg0.75 by selective laser melting [J]. Materials & Design, 2018, 140: 257−266.
[36] ROSENTHAL I, SHNECK R, STERN A. Heat treatment effect on the mechanical properties and fracture mechanism in AlSi10Mg fabricated by additive manufacturing selective laser melting process [J]. Materials Science and Engineering A, 2018, 729: 310−322.
[37] KIMURA T, NAKAMOTO T. Microstructures and mechanical properties of A356 (AlSi7Mg0.3) aluminum alloy fabricated by selective laser melting [J]. Materials & Design, 2016, 89: 1294−1301.
[38] CAO Y, LIN X, WANG Q Z, SHI S Q, MA L, KANG N, HUANG W D. Microstructure evolution and mechanical properties at high temperature of selective laser melted AlSi10Mg [J]. Journal of Materials Science & Technology, 2021, 62: 162−172.
[39] AHN S Y, MOON J, CHOI Y T, KIM E S, JEONG S G, PARK J M, KANG M, JOO H, KIM H S. A precipitation-hardened AlSi10Mg alloy fabricated using selective laser melting [J]. Materials Science and Engineering A, 2022, 844: 143164.
[40] ZHANG H, WANG Y, WANG J J, NI D R, WANG D, XIAO B L, MA Z Y. Achieving superior mechanical properties of selective laser melted AlSi10Mg via direct aging treatment [J]. Journal of Materials Science & Technology, 2022, 108: 226−235.
[41] HU J, SHI Y N, SAUVAGE X, SHA G, LU K. Grain boundary stability governs hardening and softening in extremely fine nanograined metals [J]. Science, 2017, 355: 1292−1296.
[42] LI Q G, LI G C, LIN X, ZHU D M, JIANG J H, SHI S Q, LIU F G, HUANG W D, VANMEENSEL K. Development of a high strength Zr/Sc/Hf-modified Al−Mn−Mg alloy using laser powder bed fusion: Design of a heterogeneous microstructure incorporating synergistic multiple strengthening mechanisms [J]. Additive Manufacturing, 2022, 57: 102967.
[43] UESUGI T, HIGASHI K. First-principles studies on lattice constants and local lattice distortions in solid solution aluminum alloys [J]. Computational Materials Science, 2013, 67: 1−10.

Zr 合金化引起的强晶粒细化作用同步提升激光选区熔化 AlSiMg1.4 合金的强度和塑性

耿遥祥[1]，宰春凤[1]，于 江[1]，唐 浩[2]，吕洪伟[1]，张志杰[1]

1. 江苏科技大学 材料科学与工程学院，镇江 212100；
2. 华南理工大学 国家金属材料近净成形工程技术研究中心，广州 510640

摘 要：为了提升激光选区熔化(SLM)成形高 Mg 含量 AlSiMg1.4 合金的力学性能，引入 Zr 合金化元素，并通过显微组织的分析和拉伸性能的测试研究 Zr 合金化对 SLM 成形 AlSiMg1.4 合金成形性、组织和力学性能的影响。结果表明，在不同成形工艺参数下，SLM 成形 AlSiMg1.4−Zr 合金的相对密度均超过 99.5%，表现出优异的工艺稳定性。此外，AlSiMg1.4−Zr 合金在熔体凝固过程中初生的 Al_3Zr 纳米颗粒起到了强烈的晶粒细化作用，同步提升了合金的强度和塑性。沉积态 AlSiMg1.4−Zr 合金的屈服强度、极限抗拉强度和伸长率分别为(343±3) MPa、(485±4) MPa 和(10.2±0.2)%，与 SLM 成形 AlSiMg1.4 合金和其他 Al−Si 基铝合金相比，展现出良好的强塑性协同效应。

关键词：激光选区熔化；工艺稳定性；晶粒细化；显微组织；力学性能

(Edited by Xiang-qun LI)